Acta Pharmaceutica Sinica B 2025;15(2):919–933

Chinese Pharmaceutical Association
Institute of Materia Medica, Chinese Academy of Medical Sciences

Acta Pharmaceutica Sinica B

www.elsevier.com/locate/apsb
www.sciencedirect.com

ORIGINAL ARTICLE

$P2Y_{14}R$ activation facilitates liver regeneration *via* CREB/DNMT3b/Dact-2/β-Catenin signals in acute liver failure

Mengze Zhou[a,b,†], Yehong Li[a,†], Jialong Qian[a], Xinli Dong[a], Yanshuo Guo[a], Li Yin[a], Chunxiao Liu[a], Kun Hao[a,*], Qinghua Hu[a,b,*]

[a]*State Key Laboratory of Natural Medicines, School of Pharmacy, China Pharmaceutical University, Nanjing 211198, China*
[b]*School of Life Science and Technology, China Pharmaceutical University, Nanjing 211198, China*

Received 25 June 2024; received in revised form 29 September 2024; accepted 6 November 2024

KEY WORDS

Acute liver failure;
UDP-Glucose;
$P2Y_{14}R$;
Liver regeneration;
Hepatocyte;
Partial hepatectomy;
β-Catenin;
Dact-2

Abstract Acute liver failure (ALF) is lack of broadly approved therapeutic strategy except liver transplantation. As a glycogen metabolic intermediate, UDP-glucose (UDP-G) has been considered to accelerate liver repairment. Nevertheless, the role of UDP-G and its receptor P2Y purinoceptor 14 ($P2Y_{14}R$) in ALF remains unknown. The present study aims to investigate the role and underlying mechanisms of UDP-G/$P2Y_{14}R$ axis in ALF. In this study, hepatic $P2Y_{14}R$ is significantly increased in TAA-induced and partial hepatectomy-induced ALF, while knockout of whole-body $P2Y_{14}R$ aggravates liver failure, manifested by inhibiting β-Catenin-mediated liver regeneration. Consistently, $P2Y_{14}R$ deficiency exhibits impaired liver regeneration in mice suffer partial hepatectomy. Importantly, only hepatocellular specific deletion of $P2Y_{14}R$ ($P2Y_{14}R^{flox/flox}Alb^{cre/+}$) mice shows a similar phenomenon, rather than stellate cell specific deletion of $P2Y_{14}R$ ($P2Y_{14}R^{flox/flox}Lrat^{cre/+}$) mice. Mechanistically, $P2Y_{14}R$ induction regulates methylation of Dact-2 through CREB/DNMT3b signals in hepatocytes, subsequently inhibiting the expression of Dact-2 which is a stabilizer of β-Catenin degradation complex, leading to the activation of β-Catenin -mediated liver regeneration. Interestingly, the administration of exogenous UDP-G can accelerate liver regeneration and liver function recovery after partial hepatectomy in hepatocellular carcinoma mice. Together, the findings propose an unrecognized role of $P2Y_{14}R$ in ALF and provide an effective adjuvant strategy for treatment of ALF.

*Corresponding authors.
E-mail addresses: huqh@cpu.edu.cn (Qinghua Hu), haokun@cpu.edu.cn (Kun Hao).
[†]These authors made equal contributions to this work.

Peer review under the responsibility of Chinese Pharmaceutical Association and Institute of Materia Medica, Chinese Academy of Medical Sciences.

https://doi.org/10.1016/j.apsb.2025.01.004

1. Introduction

Acute liver failure (ALF) is a rare condition involving the rapid development, progression, and worsening of liver dysfunction characterized by coagulopathy and encephalopathy, which has a high mortality rate[1]. ALF may occur under the influence of bacteria invasion, virus infection, drugs, poisons[2]. Moreover, one of the fatal complications after a major hepatectomy is postoperative liver failure, and postoperative recovery of liver function remains a challenge[3]. Current clinical drug treatment strategies are mainly etiology-based or systemic supportive therapy, and liver transplantation is still the final option for ALF patients in some cases, due to the limited therapeutic effect of these drugs[4]. The current research shows that ALF results from two distinct clinicopathologic mechanisms: (i) insufficient parenchyma, as when hepatocytes are lost through necrosis, detoxification, and synthetic requirements cannot be maintained, and (ii) hepatocyte metabolic cellular dysfunction, as seen in mitochondrial toxicity[5]. However, the molecular mechanism regulating ALF remains largely unexplored, and the discovery of key targets regulating its pathological process is of great significance for clinical drug development.

The previous studies reported that purinergic signaling played a prominent role in many aspects of health and disease, including those involving the liver[6]. Purine metabolites also have an essential role as signaling molecules in the development of disease. One previous study demonstrated that ATP activated purinergic $P2Y_2$ receptors to promote neutrophil infiltration and hepatocyte death in mice with acute liver injury[7]. Previous research has shown that UDP-glucose (UDP-G) was actively involved in regulating the occurrence and progression of liver diseases[8]. A recent study also revealed that UDP-G in hepatocytes could bind S1P to inhibit S1P-mediated cleavage of cholesterol regulatory element binding proteins SREBP, and subsequently inhibit *de novo* synthesis of fatty acids. Meanwhile, exogenous UDP-G could alleviate liver steatosis in mice by reducing ROS levels produced by oxidative decomposition of fat[9]. Moreover, UDP-G also played a potential role in liver regeneration, but the specific mechanism of action was still unclear and deserved further research[10].

The endogenous ligand UDP-G and UDP galactose activated purinergic receptor $P2Y_{14}R$ followed by the couple to Gi protein, and regulated a variety of signal transduction pathways through the intracellular cAMP level[11-13]. Therefore, we speculated that UDP-G should play a vital role in liver regeneration by activating $P2Y_{14}R$. In recent years, several studies have shown that $P2Y_{14}R$ was widely distributed in immune cells and tissue parenchymal cells and played a regulatory role in the process of acute inflammatory response. For example, the knockout of $P2Y_{14}R$ on leap cells can significantly inhibit the massive release of chemokines caused by renal ischemia reperfusion, thus reducing the inflammatory infiltration of neutrophils and monocytes in mouse kidneys[14]. Our previous study found that $P2Y_{14}R$ knockout alleviates MSU crystal-induced acute gouty arthritis by inhibiting NLRP3 inflammasome-mediated macrophage pyroptosis and promoting neutrophil death from NETosis to apoptosis by regulating the phosphorylation level of protein kinase A (PKA)[15,16]. Recent studies have also focused on the liver-disease regulatory functions of $P2Y_{14}R$[8,9]. However, the role of $P2Y_{14}R$ in the regulation of liver regeneration and ALF remains unclear.

In the present study, we reported that $P2Y_{14}R$ relied on the CREB/DNMT3b/Dact-2/β-Catenin signaling pathway to regulate liver regeneration, and thus alleviate ALF. We further found that exogenous UDP-G supplementation could promote recovery of liver function and prolong long-term survival after partial hepatectomy in hepatocellular carcinoma (HCC) model mice. In brief, our results reveal the key role of $P2Y_{14}R$ in regulating liver regeneration during ALF, providing a potential therapeutic strategy.

2. Materials and methods

2.1. Animals

All animal procedures were performed with approval by the China Pharmaceutical University Institutional Animal Care and Use Committee (approval number: 2022-01-031) and were in accordance with the Guide for the Care and Use of Laboratory Animals. $P2Y_{14}R^{-/-}$ mice (Strain No. T006700), $P2Y_{14}R^{flox/flox}$ (Strain No. T052087), *Alb*-Cre (Strain No. T003814), *Lrat*-Cre mice (Strain No. T006205) on the C57BL6/J background were purchased from Gempharmatech Co., Ltd. (Nanjing, China) at the age of 5 weeks. $P2Y_{14}R^{-/-}$ rats were obtained from Beijing Biocytogen Co., Ltd. (Beijing, China). All animal experiments were conducted with mice at the age of 6−8 weeks, and rats at the age of 6−8 weeks. All animals were kept under controlled conditions of humidity (50 ± 10%), light (12/12 h light/dark cycle), temperature (23 ± 2 °C) and given free access to a standard chow-diet (catalog No. 1010007, Xietong Bio, Nanjing, China) and water *ad libitum*. All animals were specific pathogen-free and quarantined for one week before starting the experiments. The genotypes of the mice and rats were examined *via* PCR using the total DNA derived from the tail tips. The primers used are listed in Supporting Information Table S1.

2.2. Cell lines

Human normal liver cell line LO-2 (bncc100012) was purchased from Beinachuanglian Biotechnology Company Limited. Human liver hepatocellular cell line SNU182 (ATCC, CRL-2235, male), HepG2 (ATCC, HB-8065, male) and SMMC-7721 (ATCC, H-7721, male) were obtained from ATCC (VA, USA). Cells were maintained in 5% CO_2 at 37 °C and grown in RPMI-1640 medium for LO-2 and SNU182, MEM medium for HepG2, and DMEM medium for SMMC-7721 containing 10% Fetal Bovine Serum (FBS), 2 mmol/L L-glutamine, penicillin (50 U/mL) and streptomycin (100 mg/mL) (Keygen Biotech, Nanjing, China).

2.3. Thioacetamide- (TAA-) induced acute liver failure model

Male SD rats (age, 6−8 weeks old) were attained from Huachuang Sino (Taizhou City, China). Rats fed with food and water under 12 h:12 h light-dark cycles. The random assigning of rats into two groups was undertaken as follows: control, and TAA model. PBS

was infused into rats in the control group; TAA (300 mg/kg) was intraperitoneally (i.p.) injected in the TAA model group. TAA was purchased from MCE (HY-Y0698, Shanghai, China).

2.4. Surgical procedures

The operations were carried out between 09:00 and 11:00 am under light diethyl ether anesthesia and consisted of the removal of the median and left lateral lobes of the liver. To access the liver, ventral, and midline longitudinal incisions were made to the skin and abdominal wall at the level of the organ; padded retractors were used to increase surgical visibility. The liver was externalized, and the vessels of the median, lateral, and superior right lobes of the liver were permanently ligated; subsequently, the median, left and superior right lobes were excised (approximately 30%, 50%, and 70% organ removal). The remaining lobes, the inferior right and caudate, kept moist throughout the procedure with sterile saline, were returned to their initial position within the abdominal cavity, and the field was flushed with sterile saline once again. The ventral and dorsal incisions were closed with suture and treated with 0.05% chlorhexidine gluconate followed by an alcohol swabbing. As controls, sham-operated animals were subjected to the same surgical procedure, without remission of the liver mass.

2.5. Establishment of orthotopic hepatocellular carcinoma resection model

For the establishment of an orthotopic hepatocellular carcinoma murine model, 50 μL of 5×10^5 Hepa1-6-Luc cells were injected into the left lobe of the liver of anesthetized mice. Hepa16 tumor growth was monitored by the Maestro *in vivo* imaging system (IVIS Lumina III, USA). Tumor growth was observed on Day 12 and mice were re-randomized according to tumor size. To investigate whether UDP-G could improve liver function in the early postoperative period, the left lobe of the liver was completely resected. To investigate whether UDP-G could cause HCC recurrence, the primary tumors were resected, leaving about 5% residual tumor tissue to mimic postoperative positive tumor margin.

2.6. AAV delivery into rat livers

Rats were anesthetized by intraperitoneal injection of 2% pentobarbital. A longitudinal incision was then made in the abdomen to expose the portal vein. 8×10^{11} viral particles of AAV8-GFAP-shDact2 or AAV8-GFAP-shNC in a final volume of 2 mL were injected into the portal vein with a 31-gauge needle. Four weeks after AAV infection, 70% partial hepatectomy was performed. Plasmids and AAV vectors were provided by Hanbio Biotechnology (Shanghai, China).

2.7. Serum measurements

Blood was collected and serum was separated by centrifugation at 3000 rpm for 15 min in a refrigerated bench-top centrifuge (Eppendorf AG, Hamburg, Germany). Serum alanine aminotransferase and aspartate aminotransferase levels, respectively, were determined using the alanine aminotransferase (ALT) and aspartate aminotransferase (AST) kits. For measurement of alkaline phosphatase and direct bilirubin (DBIL) kit in serum, alkaline phosphatase and DBIL kit were used. All kits were purchased from Nanjing Jiancheng Bioengineering Institute (Nanjing, China).

2.8. Histology

Excised liver samples were fixed in 4% (*w*/*v*) neutrally buffered formalin, embedded in paraffin and cut into 3 mm consecutive slices for hematoxylin and eosin (H&E) and staining of Ki67. Immunohistochemical staining was performed under standardized conditions on a Discovery XT automated stainer (Ventana Medical Systems) using monoclonal rabbit anti-Ki67 (1:250, Abcam) as a primary antibody and goat anti-rabbit, biotinylated (1:750) (Vector Laboratories) as secondary antibody. The stained tissue sections were scanned with a microscope (Olympus Optical, BX53).

2.9. Immunofluorescence

The liver tissue was processed for immunofluorescence. The liver slices were washed third with PBS and blocked with 0.3% Triton X-100 in 5% BSA (Beyotime, Shanghai, China) for 2 h at room temperature. Then slices were incubated with primary antibodies of β-Catenin (1:50, ab25898, Abcam), Dact-2 (1:50, ab25898, Abcam), and *N*-P-β-Catenin (1:50, ab25898, Abcam) at 5% BSA overnight at 4 °C. Liver slices were washed six times with PBS before incubating with Donkey Anti-Rabbit IgG (H+L) Antibody, Alexa Fluor 488 (1:1000, A-21206, Invitrogen) and Donkey Anti-Mouse IgG (H+L) Antibody, Alexa Fluor 555 (1:1000, A-31570, Invitrogen) for 1 h at 37 °C in 5% BSA, then washed five times with PBS. Cell images were acquired on BX53 confocal microscope (Olympus, Japan).

2.10. Western blot

Liver or cells protein lysates were extracted using RIPA buffer (Beyotime, Shanghai, China), and the protein concentration was measured using the BCA assay (Beyotime, Shanghai, China). Proteins were separated by electrophoresis on 4%−20% Tris gels (Invitrogen, CA, USA) and transferred to 0.45-mm nitrocellulose membranes (Millipore, Bedford, USA). The membranes were blocked for 1 h at room temperature in Tris-buffered saline/0.1% Tween 44 (TBST) containing 5% (*w*/*v*) nonfat milk and then incubated with the primary antibody in TBST containing 5% (*w*/*v*) BSA at 4 °C overnight. The membranes were then incubated with the appropriate secondary antibody coupled to horseradish peroxidase, and proteins were detected by Image ChemiScope 6000 software (CLiN, Shanghai, China). Cultured cells were lysed in 2 × loading buffer (Beyotime, Shanghai, China), heated at 100 °C for 5 min, and then electrophoresed and immunoblotted as above. The antibodies used included β-Catenin (bs-1165R, Bioss, Beijing, China), *N*-P-β-Catenin (D13A1, CST, Danvers, USA), p-GSK3β (bs-5368R, Bioss), GSK3β (bsm-33294M, Bioss), LEF1 (bsm-51694M, Bioss), c-Myc (bsm-51652M, Bioss), Cyclin D1 (bsm-52046R, Bioss), CyclinB1 (AF6168, Affinity, China), β-actin (bs-0061R, Bioss), Dact-2 (PA5-20629, Thermo), P-MLKL (AF7443, Affinity), MLKL (66675-1-1g, Proteintech, Wuhan, China), P-RIP1 (AF2398), RIP1 (17519-1-AP, Proteintech), P-RIP3 (AF2398, Affinity), RIP3 (17563-1-AP, Proteintech), P-STAT3 (AF3293, Affinity), STAT3 (10253-2-AP, Proteintech), IL-6 (DF6087, Affinity), IL-22 (DF8343, Affinity) and rabbit anti-mouse IgM/HRP antibody (bs-0368R-HRP, Bioss).

2.11. RNA isolation and quantitative RT-PCR

Total RNA was extracted from liver tissue or cultured cells using TransZol UP (ET111-01, TransGen Biotech, Beijing, China). The

quality and concentration of the RNA were assessed by absorbance at 260 and 280 nm using a SpectraMax iD3 (Molecular Devices, USA). cDNA was synthesized from 0.5 to 1 mg RNA using TransScript® All-in-One First-Strand cDNA Synthesis SuperMix for qPCR (One-Step gDNA Removal) (AT341-02, TransGen Biotech, Beijing, China). Quantitative RT-PCR was performed with a QuantStudio 1 appliedbiosystems (Thermo Scientific, Waltham, USA) using PerfectStart Green qPCR SuperMix (+Dye II) (AQ602-22, TransGen Biotech). The primer sequences (Generay Biotech Co., Ltd., Shanghai, China) are listed in Supporting Information Table S2.

2.12. Metabolite analysis

To assess hepatic UDP-G level, liver tissues of rats were collected and frozen in liquid nitrogen for LC−MS analysis. The Vanquish UHPLC system (ThermoFisher) was combined with an Orbitrap Q ExactiveTM HF-X mass spectrometer (ThermoFisher) for UHPLC−MS/MS analyses at Gene Denovo Biotechnology Co.

2.13. RNA-sequencing

For RNA-seq of liver from mice, total RNA (50−100 ng) was prepared for sequencing using trizol reagent kit (Invitrogen) according to the manufacturer's protocol. RNA quality was assessed on an Agilent 2100 Bioanalyzer (Agilent Technologies, Palo Alto, CA, USA) and checked using RNase free agarose gel electrophoresis. After total RNA was extracted, eukaryotic mRNA was enriched by Oligo (dT) beads. Then the enriched mRNA was fragmented into short fragments using fragmentation buffer and reverse transcripted into cDNA with random primers. Second-strand cDNA was synthesized by DNA polymerase I, RNase H, dNTP and buffer. Then the cDNA fragments were purified with QiaQuick PCR extraction kit (Qiagen, Venlo, The Netherlands), end repaired, poly(A) added, and ligated to Illumina sequencing adapters. The ligation products were size selected by agarose gel electrophoresis, PCR amplified, and sequenced using Illumina Novaseq6000 by Gene Denovo Biotechnology Co. (Guangzhou, China).

2.14. Cell counting Kit-8 (CCK-8) assay

Evaluation of cell survival rates was carried out using the CCK-8 assay (Biosharp Life Science, Hefei, China). Seeding of 1×10^4 cells into 96-well plates was conducted. After 24 h of culture, different doses of UDP-G (10, 20, 50, 100, and 200 μmol/L) were added separately. Incubation of each well was undertaken with the assistance of 10 μg CCK-8 in the dark (0.5, 1, 1.5, 2, 2.5, 3, 3.5, and 4 h). We also could measure absorbance (450 nm) *via* a SpectraMax iD3 (Molecular Devices, San Jose, USA).

2.15. Plasmid transfection

To overexpress $P2Y_{14}R$ ($P2Y_{14}R$-OE), LO-2 cells were plated at a density of 5×10^5 per well and transfected with PEX3 plasmid (GenePharma, Shanghai, China) for 48 h using Lipofectamine 3000 (Thermo Scientific) according to the manufacturer's instructions.

2.16. Methylation specific PCR (MSP)

Genomic DNA was prepared by the proteinase K method using FastPure Cell/Tissue DNA Isolation Mini Kit (DC102, Vazyme, Nanjing, China). For DNA bisulfite modification, we used the EpiTect Fast DNA Bisulfite kit (59824, QIAGEN, Hilden, German) according to the manufacturer's protocol. The methylated CpG islands in the promoter region of Dact-2 were predicted by MethPrimer software (The Li Lab, urogene.org). Methylation primers were designed according to genomic sequences around transcription start sites (TSS) and synthesized to detect methylated (M) and unmethylated (U) alleles. Methylation primers for Dact-2 are shown in Supporting Information Table S3. Amplified total DNA was subjected to electrophoresis on a 2% agarose gel, and then visualized by ethidium bromide staining.

2.17. Chromatin immunoprecipitation (ChIP)-qPCR

Chromatin immunoprecipitation was conducted following the instruction of SimpleChIP® Plus Enzymatic Chromatin IP Kit (Magnetic Beads) (#9005, Cell Signaling Technology, Danvers, USA). Signals obtained from each immunoprecipitation were presented by percent of the total input chromatin. Potential DNMT3b binding sites in the promoter region of target genes were predicted using the JASPAR website (https://jaspar.genereg.net/) and verified by real-time PCR. Primers used in the ChIP assay are listed in Extended Data Table S2.

2.18. Kaplan−Meier survival analysis

The prognostic value of $P2Y_{14}R$ in HCC was studied in the Kaplan−Meier plotter (http://kmplot.com/analysis/) by displaying overall survival, progression-free survival, recurrence free survival and disease-specific survival. The Kaplan−Meier survival curve, log-rank *P*-value, and hazard ratio (HR) with 95% confidence intervals between $P2Y_{14}R$ high expression and low expression groups were plotted and calculated as previously described[17].

2.19. Statistical analysis

All data were expressed as the mean ± standard deviation (SD). Data were tested for normality prior to the use of parametric tests. For the comparison of 2 groups, unpaired two-tailed t was used for normally distributed data, Mann−Whitney tests for non-normally distributed data. In experiments with more than 2 groups one-way ANOVA with *post hoc* Sidak test for normally distributed data and Kruskal−Wallis with Dunn *post hoc* test for not normally distributed data. Analysis was performed using GraphPad Prism version 9 for Win.

All of the data associated with this study can be found in the paper or the Supporting Information. The raw sequencing data from this study have been deposited in the Genome Sequence Archive in BIG Data Center (http://bigd.big.ac.cn/), Beijing Institute of Genomics (BIG), Chinese Academy of Sciences, under the accession number: CRA014618.

3. Results

3.1. Deletion of *P2Y$_{14}$R* exacerbates ALF manifested the inhibition of liver regeneration pathways

To explore the regulatory role of $P2Y_{14}R$ in ALF, we analyzed the expression of $P2Y_{14}R$ from GEO databases (GSE237801, GSE53082, GSE15239, GSE215423, GSE181761). The result shows that the expression levels of *P2ry$_{14}$* were increased in TAA-induced and partial hepatectomy-induced ALF (Fig. 1A). To

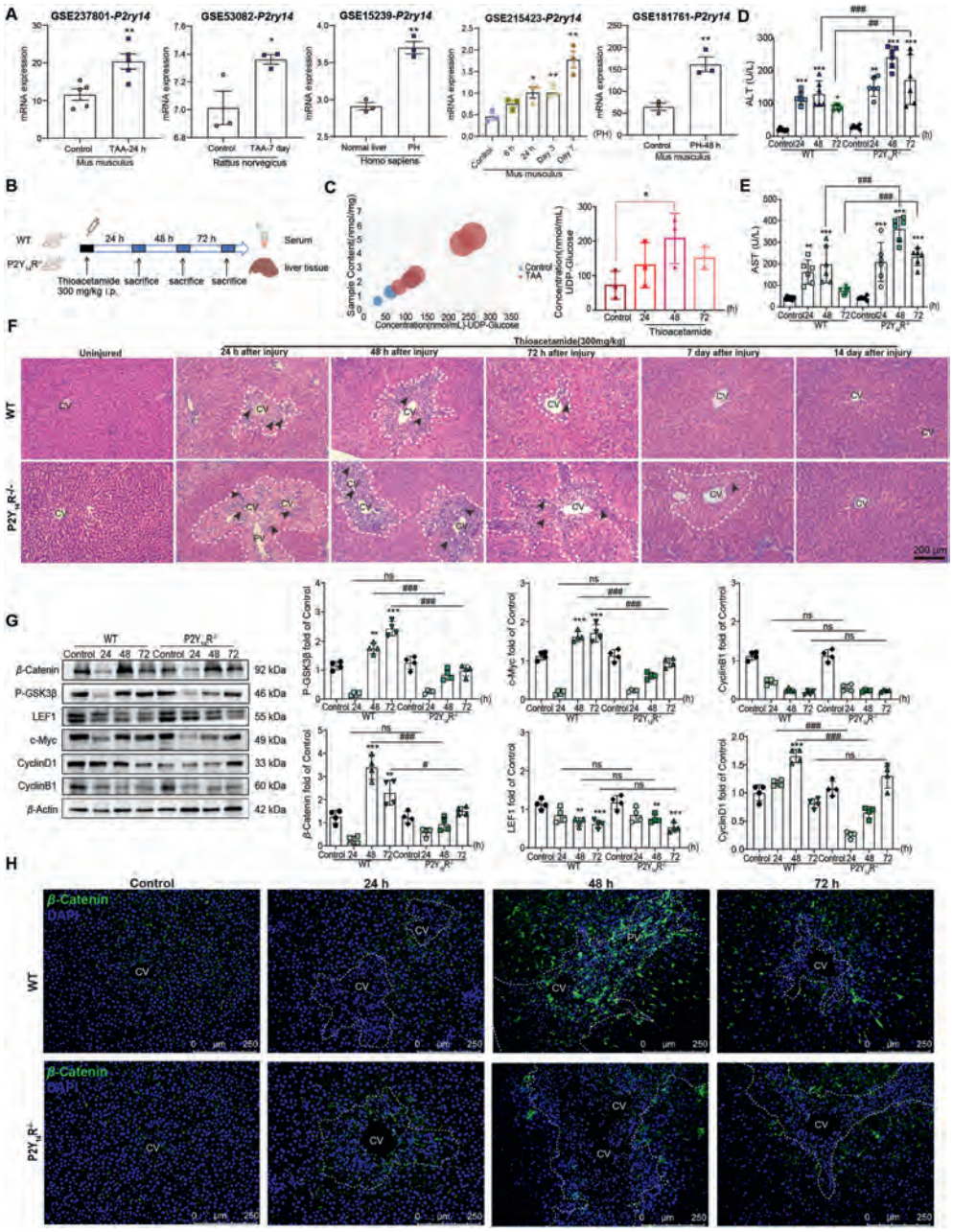

Figure 1 P2Y$_{14}$R knockout aggravates TAA-induced ALF by inhibiting β-Catenin signaling. (A) *P2ry14* expression in the liver tissue after TAA injection or hepatectomy from GEO database, using datasets GSE237801 (n = 5 biological replicates), GSE53082 (n = 3 biological replicates), GSE15239 (n = 3 biological replicates), GSE215423 (n = 3 biological replicates), GSE181761 (n = 3 biological replicates). (B) Schematic illustrating construction of ALF model in rats induced by TAA. (C) Variation tendency of UDP-G concentrations in liver tissues at different time points, n = 3 biological replicates. (D, E) The levels of ALT and AST in serum, n = 6 rats per group. (F) Representative images of HE staining of liver sections from WT rats and P2Y$_{14}$R$^{-/-}$ rats treated with 300 mg/kg TAA. Scale bar, 200 μm. (G) Protein expressions of key factors involved in β-Catenin signaling. p-, phosphorylated, n = 4 rats per group. (H) Representative images of immunofluorescent staining of β-Catenin (green) in liver sections. The nuclei were labeled with DAPI (blue). Scale bar, 250 μm. Data are shown as the mean ± SD, $^{*}P < 0.05$, $^{**}P < 0.01$, $^{***}P < 0.001$ *versus* Control group; $^{\#}P < 0.05$, $^{\#\#}P < 0.01$, $^{\#\#\#}P < 0.001$ *versus* WT group. ns, no significance; CV, central vein.

elucidate the physiological functions of P2Y$_{14}$R, we generated rats of P2Y$_{14}$R deficient in the whole body (P2Y$_{14}$R$^{-/-}$) and induced ALF by TAA (Supporting Information Fig. S1A, Fig. 1B). We detected the changes of UDP-G at different time nodes. The results show that the content of UDP-G increased significantly and reached a peak at 48 h after TAA-induced ALF (Fig. 1C). There were slight levels of ALT and AST in the control livers, which were significantly higher in P2Y$_{14}$R$^{-/-}$ rats compared with wild type (WT) rats (Fig. 1D and E). Consistent with this finding, the liver lobular structure of WT and P2Y$_{14}$R$^{-/-}$ rats intraperitoneally injected with PBS appeared histologically normal, characterized by neatly arranged hepatic cords and clearly visible hepatic

sinuses. However, 24 h after TAA injection in WT rat liver, hepatocyte necrosis and disordered hepatic cord arrangement were observed along with a minor infiltration of monocytes and red blood cells. The extent of injury reached its peak at 48 h, followed by a gradual decrease in inflammatory infiltration after 72 h. Subsequently, the area of liver cell injury reduced progressively until complete repair was achieved after 7 days. By contrast, the deletion of $P2Y_{14}R$ exacerbated TAA-induced liver injury (Fig. 1F).

We then examined whether $P2Y_{14}R$ deficiency affected compensatory regeneration of the liver. The levels of protein associated with necrosis, including p-MLKL, p-RIP1 and p-RIP3 protein expressions in the WT and $P2Y_{14}R^{-/-}$ rat livers were almost unchanged (Fig. S1B). Considering the extremely strong regenerative capacity of the liver, we examined the liver repair related proteins IL-6, IL-22 and STAT3. The results show that after TAA induction, the expression of IL-6 was significantly increased, the expression of IL-22 was significantly decreased, and the level of p-STAT3 was not significantly changed. However, there were no significant changes in their expression after $P2Y_{14}R$ knockout (Fig. S1C). As $P2Y_{14}R$ knockout had no significant effect on the protein expression level of necroptosis signaling pathway in TAA-induced ALF, the study further investigated whether the aggravation of liver failure was through the influence of post-injury repair. Whereas the expressions of liver regeneration related proteins β-Catenin, p-GSK3β, c-Myc and CyclinD1 were elevated at 24 h and the increased levels were maintained throughout the observation period (48 h) and 72 h. The expressions of β-Catenin, p-GSK3β, c-Myc and CyclinD1 protein were greatly reduced in the livers of $P2Y_{14}R^{-/-}$ rats, but LEF1 and CyclinB1 protein expressions were not affected in either quiescent or regenerating livers (Fig. 1G). Moreover, the results of immunofluorescence showed that β-Catenin expression in the liver around the damaged central vein increased gradually at 24 h after TAA induction, and the expression was the strongest at 48 h while decreased at 72 h. However, $P2Y_{14}R$-deficient livers decreased the expression level of β-Catenin (Fig. 1H, Fig. S1D). These findings suggest that $P2Y_{14}R$ knockout aggravated TAA-induced ALF by inhibiting β-Catenin-mediated liver regeneration and delaying the repair of damaged liver.

3.2. *Deficiency of $P2Y_{14}R$ aggravates ALF after 70% hepatectomy by suppressing liver regeneration*

To examine whether $P2Y_{14}R$ has a direct effect on liver regeneration, we performed 70% partial hepatectomy on WT, $P2Y_{14}R^{+/-}$ and $P2Y_{14}R^{-/-}$ rats respectively (Fig. 2A). We observed increased serum levels of ALT and AST of partial hepatectomy group compared with sham group, and the serum levels of ALT and AST of $P2Y_{14}R^{+/-}$ and $P2Y_{14}R^{-/-}$ rats showed a dramatic increase than WT rats (Fig. 2B). We next found that the liver regeneration rate of $P2Y_{14}R^{+/-}$ and $P2Y_{14}R^{-/-}$ rats had a reduction after 70% hepatectomy compared with WT rats (Fig. 2C). Moreover, the expression of $Ki67^{+}$ cells in the liver of WT rats was significantly higher than that of $P2Y_{14}R^{+/-}$ and $P2Y_{14}R^{-/-}$ rats after 70% hepatectomy (Fig. 2D). Interestingly, we found that the protein level of Non-phospho (Active) β-Catenin (*N*-P-β-Catenin) and β-Catenin were lowered after 70% hepatectomy in $P2Y_{14}R^{-/-}$ rats compared with WT rats. We obtained that $P2Y_{14}R^{-/-}$ rats after 70% hepatectomy had decreased expressions of p-GSK3β, Cyclin D1 and c-Myc protein compared with WT rats (Fig. 2E). These results suggest that whole-body knockout of $P2Y_{14}R$ exacerbated acute liver injury by inhibiting the β-Catenin -mediated liver regeneration pathway.

3.3. *$P2Y_{14}R$ regulates liver regeneration dependent on Dact-2 in rat model after 70% hepatectomy*

To elucidate the mechanism of $P2Y_{14}R$ regulating liver regeneration, we performed RNA-sequencing in WT and $P2Y_{14}R^{-/-}$ rats after 70% hepatectomy. It is important to note that, Dact-2 of disheveled family genes has the most obvious differences between WT rats with $P2Y_{14}R^{-/-}$ rats (Fig. 3A). Moreover, the results show that the expression of Dact-2 in liver of $P2Y_{14}R$ knockout rats was significantly increased compared with WT rats (Fig. 3B). Immunofluorescence stain verified the upregulation of Dact-2 in $P2Y_{14}R$ knockout rats compared with WT rats after partial hepatectomy (Fig. 3C). We also obtained a similar result in the TAA-induced ALF model (Supporting Information Fig. S2). These data reveal that $P2Y_{14}R$ knockout inhibited liver regeneration through Dact-2.

The expression of Dact-2 is essential for disease through Wnt/β-Catenin signaling pathway[18-20]. To address whether $P2Y_{14}R$ regulated hepatocyte regeneration depended on Dact-2, we injected Dact-2-shRNA-loaded AAV8 virus into rats with $P2Y_{14}R^{-/-}$ background to construct Dact-2-knockdown rats. The empty AAV8 vector was used as a blank control (NC-shRNA). After 4 weeks, the expression of Dact-2 protein was significantly inhibited (Fig. 3D and E). In the Dact-2-knockdown rat model, we observed an increase in liver regeneration rate compared with NC-shRNA-loaded rats (Fig. 3F). Moreover, we observed that the knockdown of Dact-2 did not affect Ki67 expression in liver without surgical treatment. Following partial hepatectomy, Ki67 expression was markedly increased and increased further when Dact-2 was knockdown (Fig. 3G and H). Then we further confirmed the role of Dact-2 in liver regeneration, the results show that the expression of *N*-P-β-Catenin and β-Catenin were increased in $P2Y_{14}R^{-/-}$ rats after Dact-2 shRNA injection (Fig. 3I). The *N*-P-β-Catenin, β-Catenin, p-GSK3β and cyclinD1 protein expression levels were increased in $P2Y_{14}R^{-/-}$ rats after Dact-2 shRNA injection (Fig. 3J). All the above results indicate that Dact-2 played a key role in $P2Y_{14}R$-mediated regulation of liver regeneration.

3.4. *Hepatocyte specific knockout of $P2Y_{14}R$ inhibits liver regeneration*

Liver regeneration is an extremely complex process involving many kinds of cells, including hepatic stellate cells and hepatocytes[21]. $P2Y_{14}R$ is highly expressed in hepatic stellate cells and its role in hepatic fibrosis has been elucidated[8]. Besides, the hepatocyte is a major functional cell type of liver and is a peculiar cell with remarkable regenerative capacity[22]. So hepatic stellate cell $P2Y_{14}R$-specific knockout ($P2Y_{14}R^{flox/flox}Lrat^{cre/+}$) mice and hepatic $P2Y_{14}R$-specific knockout ($P2Y_{14}R^{flox/flox}Alb^{cre/+}$) mice were used to investigate liver regeneration after partial hepatectomy (Fig. 4A). We observed a reduced rate of liver regeneration in $P2Y_{14}R^{-/-}$ mice compared to WT mice (Fig. 4B). However, $P2Y_{14}R^{flox/flox}Lrat^{cre/+}$ mice showed no significant difference in liver regeneration rate compared with $P2Y_{14}R^{flox/flox}$ mice (Fig. 4C). Then, we performed 70% hepatectomy in $P2Y_{14}R^{flox/flox}Alb^{cre/+}$ mice and $P2Y_{14}R^{flox/flox}$ mice (Supporting Information Fig. S3A). Unexpectedly, we found that $P2Y_{14}R^{flox/flox}Alb^{cre/+}$ mice had 100% mortality at 24 h. Therefore, we tried 30% and 50% partial hepatectomy and found a significant reduction in

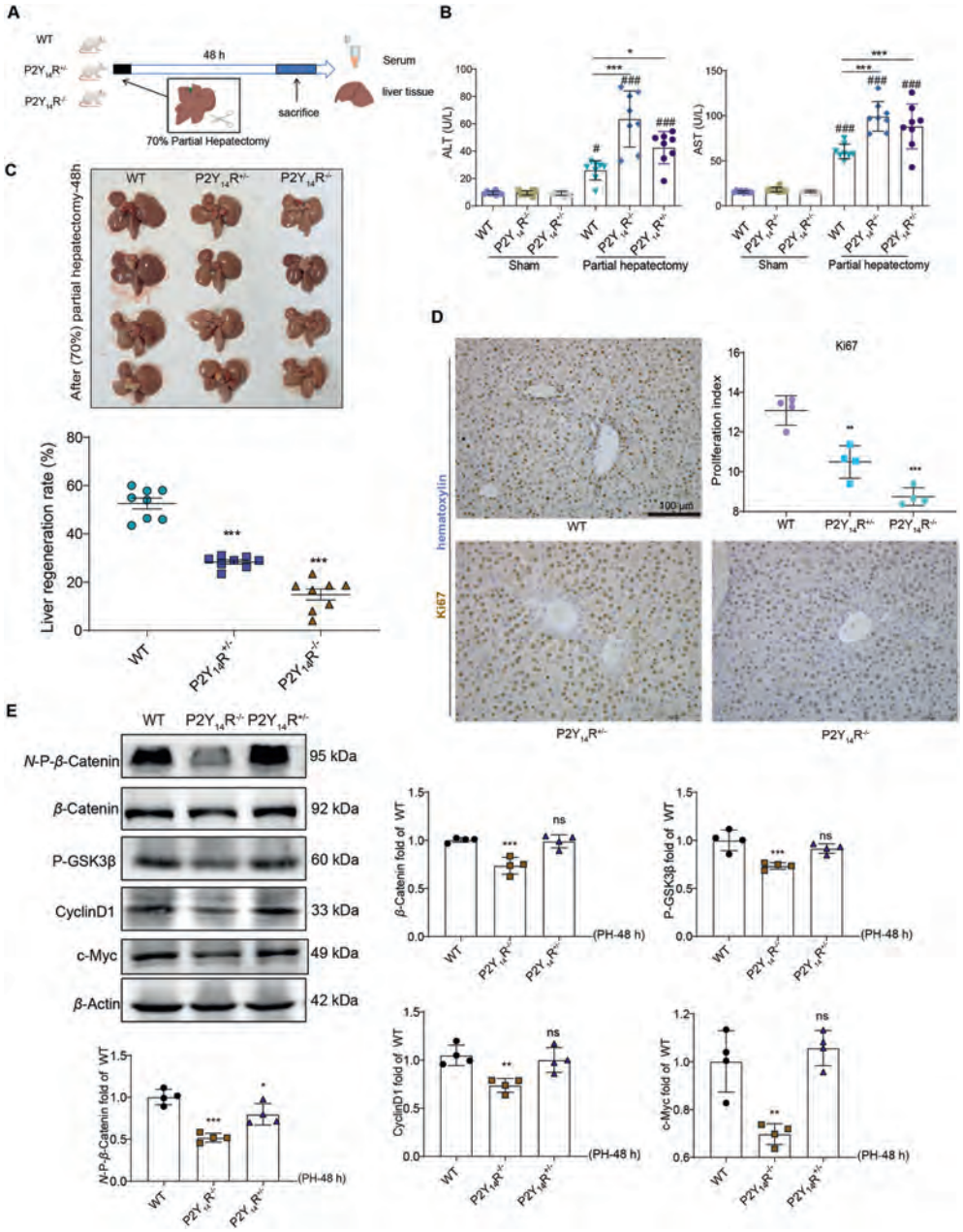

Figure 2 Deficiency of P2Y$_{14}$R inhibits liver regeneration after partial hepatectomy. (A) Schematic illustrating construction of 70% partial hepatectomy model. (B) ALT and AST levels in the serum, $n = 8$ rats per group. (C) Gross morphology of livers and liver regeneration rate in rats after 70% hepatectomy, $n = 8$ rats per group. (D) Representative images of immunohistochemistry staining showing Ki67 expression, $n = 4$ rats per group. Scale bar, 100 μm. (E) Protein expressions of key factors involved in β-Catenin signaling in the livers of rats, $n = 4$ rats per group. Data are shown as the mean ± SD, $^{*}P < 0.05$, $^{**}P < 0.01$, $^{***}P < 0.001$ *versus* WT group; $^{\#}P < 0.05$, $^{\#\#}P < 0.01$, $^{\#\#\#}P < 0.001$ *versus* Sham group. ns, no significance.

mortality (Fig. 4D). At the same time, lower liver regeneration rates were observed in the P2Y$_{14}$R$^{flox/flox}$*Alb*$^{cre/+}$ mice compared to the P2Y$_{14}$R$^{flox/flox}$ mice (Fig. 4E). These results indicate that P2Y$_{14}$R knockout in hepatocytes could significantly inhibit the regeneration after ALF.

To determine whether P2Y$_{14}$R interfered with β-Catenin mediated liver regeneration by affecting the expression of Dact-2 in P2Y$_{14}$R$^{flox/flox}$*Alb*$^{cre/+}$ mice, we detected the associated protein expressions. The results show that the expressions of p-GSK3β, c-Myc, CyclinD1 and *N*-P-β-Catenin were significantly reduced in P2Y$_{14}$R$^{flox/flox}$*Alb*$^{cre/+}$ mice compared with P2Y$_{14}$R$^{flox/flox}$ mice. However, the level of Dact-2 in P2Y$_{14}$R$^{flox/flox}$*Alb*$^{cre/+}$ mice was significantly higher than that in P2Y$_{14}$R$^{flox/flox}$ mice (Fig. 4F–I, Fig. S3B). In addition, there was a lower expression of *N*-P-β-Catenin and β-Catenin in P2Y$_{14}$R$^{flox/flox}$*Alb*$^{cre/+}$ mice compared to P2Y$_{14}$R$^{flox/flox}$ mice after ALF. In contrast, there was higher expression of Dact-2 in P2Y$_{14}$R$^{flox/flox}$*Alb*$^{cre/+}$ mice (Fig. 4J, Supporting Information Fig. S4). These results demonstrate that hepatocytes P2Y$_{14}$R regulated liver regeneration after ALF through the intervention of β-Catenin by Dact-2.

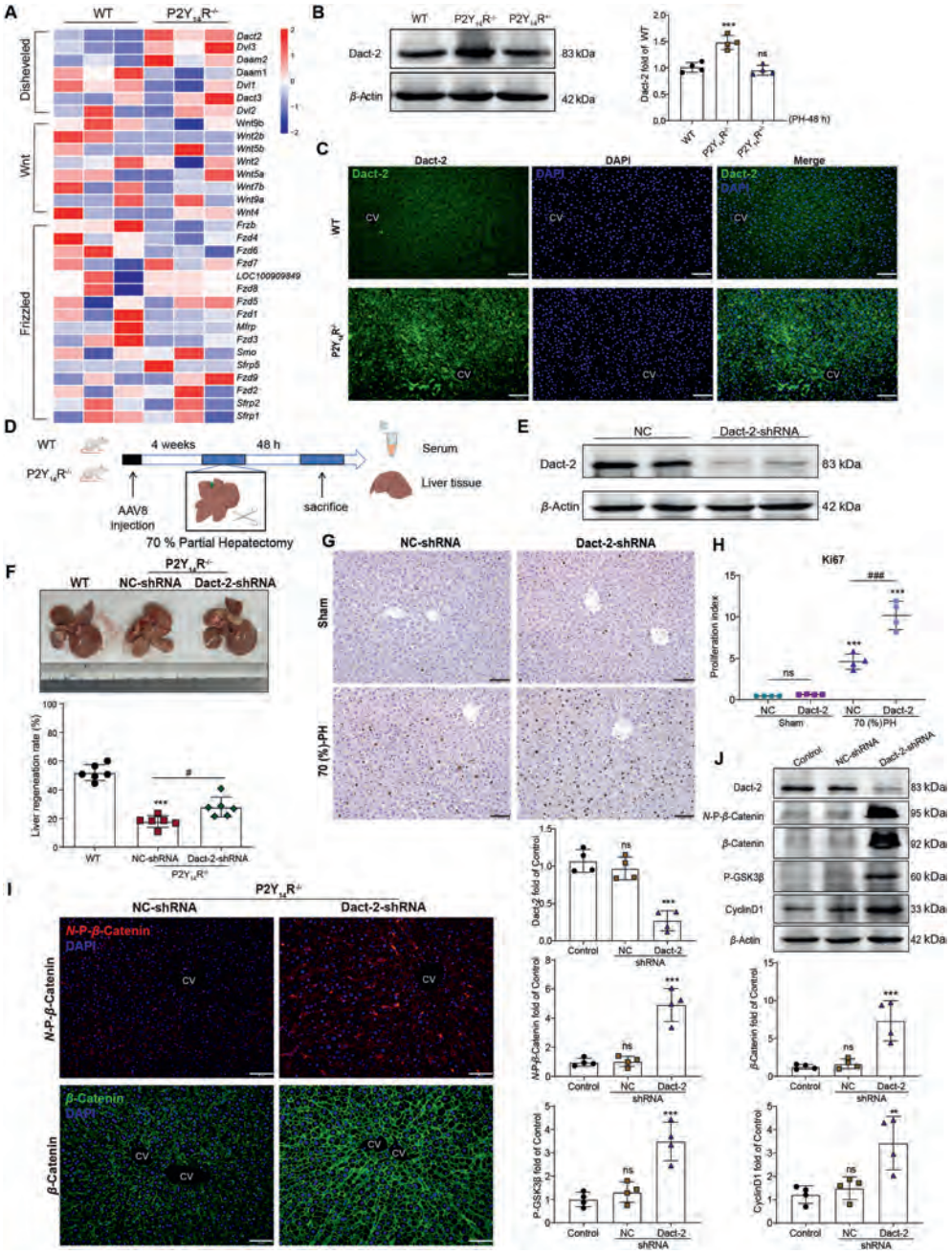

Figure 3 P2Y$_{14}$R regulates liver regeneration signaling dependent on Dact-2 in 70% hepatectomy model. (A) Differential expression analysis of genes involved in β-Catenin regulatory signals. (B, C) Representative Western blots ($n = 4$ rats per group) (B) and images of immunofluorescent staining (C) of Dact-2 in the livers. (D) Schematic illustrating schedule of AAV8 injection and hepatectomy. (E) Protein expression of Dact-2 in livers, $n = 4$ rats per group. (F) Gross morphology of livers and liver regeneration rate, $n = 6$ rats per group. (G, H) Representative images of immunohistochemical staining showing Ki67 expression (G) and proliferation index (H), $n = 4$ rats per group. Scale bar, 100 μm. (I) Representative images of immunofluorescent staining of *N*-P-β-Catenin and β-Catenin in liver sections. Scale bar, 50 μm. (J) Protein expressions of key factors involved in Dact-2/β-Catenin signaling, $n = 4$ rats per group. Data are shown as the mean ± SD, $^{*}P < 0.05$, $^{**}P < 0.01$, $^{***}P < 0.001$ *versus* Control group; $^{\#}P < 0.05$, $^{\#\#}P < 0.01$, $^{\#\#\#}P < 0.001$ *versus* NC-shRNA group. ns, no significance; CV, central vein.

3.5. UDP-G activates P2Y$_{14}$R to regulate Dact-2 methylation level in a DNMT3b-dependent manner

Previous studies showed that the proliferation ability of normal liver cell lines and tumor liver cell lines may be different[23]. To explore the mechanism of P2Y$_{14}$R regulating Dact-2, we stimulated human normal liver cell line LO-2 and human liver cancer cell line HepG2 with different concentrations of UDP-G (10, 20, 50, 100, and 200 μmol/L) at different time (24, 48, and 72 h). Compared with the control group, LO-2 significantly proliferated under 20 μmol/L UDP-G stimulation at 24, 48 and 72 h, while HepG2 cells were significantly proliferated at 48 h under the concentration of 20 μmol/L (Fig. 5A). Therefore, we choose 20 μmol/L UDP-G for the subsequent administration. The

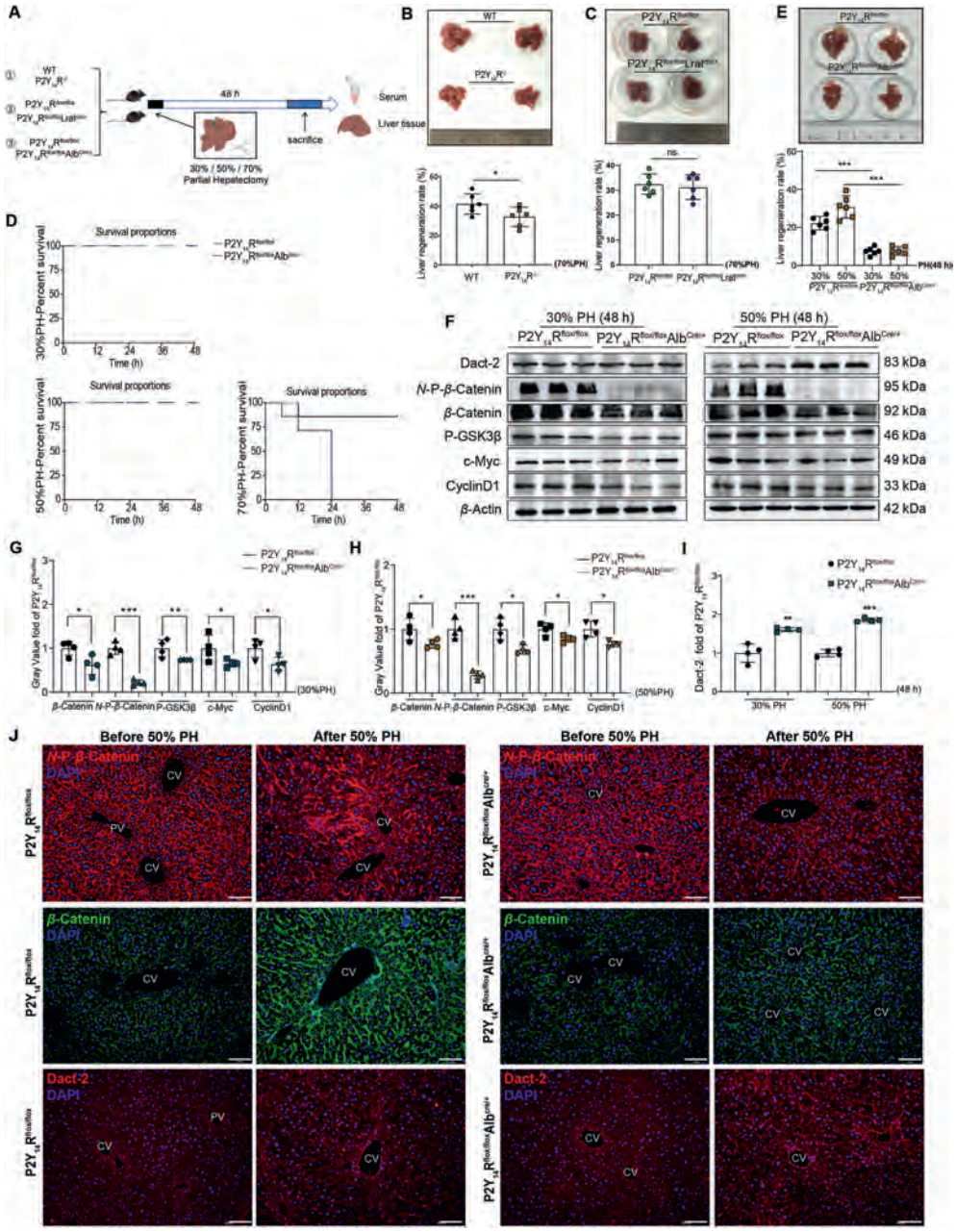

Figure 4 Hepatocyte specific knockout of P2Y$_{14}$R inhibits liver regeneration after partial hepatectomy. (A) Schematic illustrating construction of mice partial hepatectomy model. (B, C) Gross morphology of livers and liver regeneration rate in P2Y$_{14}$R$^{-/-}$ (B) and P2Y$_{14}$R$^{flox/flox}$ *Lrat*$^{cre/+}$ mice (C) after 70% hepatectomy, $n = 6$ mice per group. (D) Survival proportions of P2Y$_{14}$R$^{flox/flox}$ and P2Y$_{14}$R$^{flox/flox}$*Alb*$^{cre/+}$ mice after resection of different proportions of the liver, $n = 10$ mice per group. (E) Gross morphology of livers and liver regeneration rate in P2Y$_{14}$R$^{flox/flox}$ and P2Y$_{14}$R$^{flox/flox}$*Alb*$^{cre/+}$ mice after 30% and 50% hepatectomy, $n = 6$ mice per group. (F–I) Protein expressions of key factors involved in Dact-2/β-Catenin signaling in the livers of mice after hepatectomy, $n = 4$ mice per group. (J) Representative images of immunofluorescent staining of *N*-P-β-Catenin, β-Catenin and Dact-2 in liver sections from mice subjected to 50% hepatectomy. Scale bar, 50 μm. Data are shown as the mean ± SD, $^*P < 0.05$, $^{**}P < 0.01$, $^{***}P < 0.001$. ns, no significance; CV, central vein.

methylation of the Dact-2 promoter is the key factor causing the decreased expression[24]. We therefore investigated whether P2Y$_{14}$R regulated the methylation of Dact-2. We predicted the CpG islands of the Dact-2 promoter region through MethPrimer software (Supporting Information Fig. S5) and designed primers (Table S3).

To detect the methylation level of Dact-2 promoter by methylation-specific PCR, we extracted DNA from human hepatocellular carcinoma cell lines (SNU182, HepG2 and SMMC-7721) and normal stem cell lines (LO-2). We observed that the Dact-2 promoter was highly methylated in human hepatocellular carcinoma cell lines, while the Dact-2 promoter in LO-2 was unmethylated (Fig. 5B). Meanwhile, the methylation level of Dact-2 promoter in LO-2 cells transfected with P2Y$_{14}$R over-expressing plasmid (P2Y$_{14}$R-OE) was significantly increased compared with blank plasmid (Vector) (Fig. 5C). DNMT catalyzes and maintains methylation, among which DNMT1, DNMT3a and

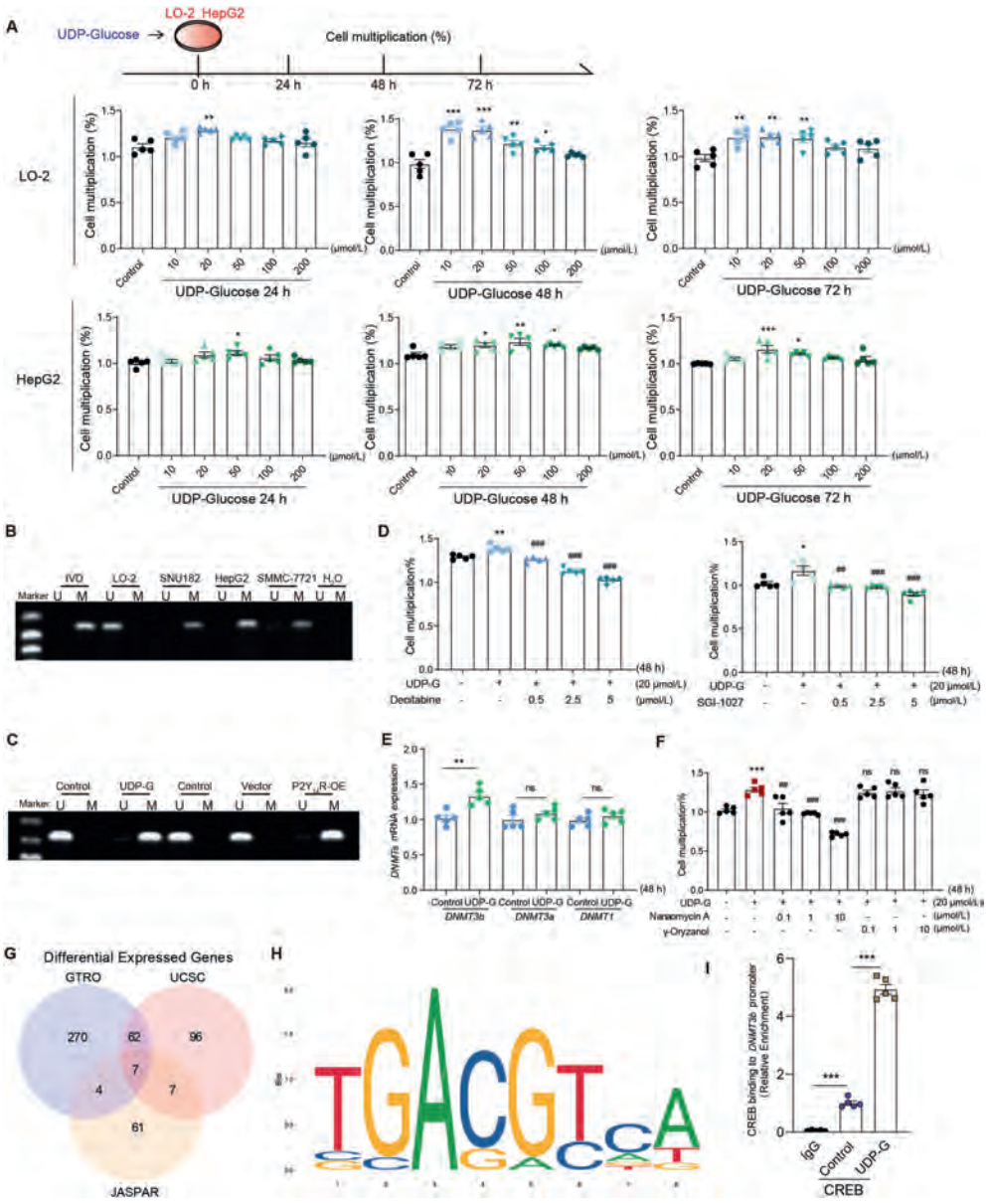

Figure 5 UDP-G activates $P2Y_{14}R$ to regulate Dact-2 methylation level depending on DNMT3b. (A) Proliferation state of LO-2 and HepG2 cells exposed to UDP-G, $n = 5$ biological replicates. (B, C) Detection of intracellular methylation levels in different cell lines or after different treatments. (D) Effects of DNMT broad spectrum inhibitors on proliferation of LO-2 cells exposed to UDP-G, $n = 5$ biological replicates. (E) mRNA expression of *DNMT* subtypes in LO-2 cells stimulated by UDP-G, $n = 5$ biological replicates. (F) Effect of specific inhibitors of DNMT on the proliferation of LO-2 cells, $n = 5$ biological replicates. (G) Venn diagrams of transcription factors bound to *DNMT3b* in GTRO, UCSC and JASPAR databases. (H) CREB-binding motifs. (I) ChIP with anti-CREB of the regions containing the CREB binding sites on the *DNMT3b* gene promoter in LO-2 cells stimulated by UDP-G, $n = 5$ biological replicates. Data are shown as the mean ± SD, $^{*}P < 0.05$, $^{**}P < 0.01$, $^{***}P < 0.001$. ns, no significance.

DNMT3b have methyl transfer activity[25,26]. Therefore, we used broad-spectrum DNMT inhibitors decitabine, SGI-1027 and observed that UDP-G stimulation significantly increased the proliferation of LO-2 cells, while the intervention of decitabine and SGI-1027 reduced cell proliferation (Fig. 5D). Then, mRNA expression of each subtype was detected after 48 h of UDP-G stimulation. The results show that the expression of *DNMT3b* was significantly increased (Fig. 5E). Further, we found that selective inhibitor Nanaomycin A of DNMT3b significantly inhibited the proliferation of LO-2 cells, while selective inhibitor γ-oryzanol of DNMT3a and DNMT1 had no significant inhibitory effect (Fig. 5F). These results suggest that $P2Y_{14}R$ regulation of Dact-2 expression might depend on DNMT3b.

To explore the upstream molecular mechanisms of DNMT3b, we used three online transcription factors prediction websites (GTRO, UCSC and JASPAR) to predict potential transcription factors bound to the promoter of DNMT3b. We found 7 common transcription factors and focused on the cAMP-response element binding protein (CREB) among them (Fig. 5G). In our previous study, CREB was the downstream pathway of cAMP/PKA signal activated by $P2Y_{14}R$ deficiency in neutrophils[27]. Therefore, we explored the binding of CREB to DNMT3b in hepatocytes. We used the JASPAR (threshold

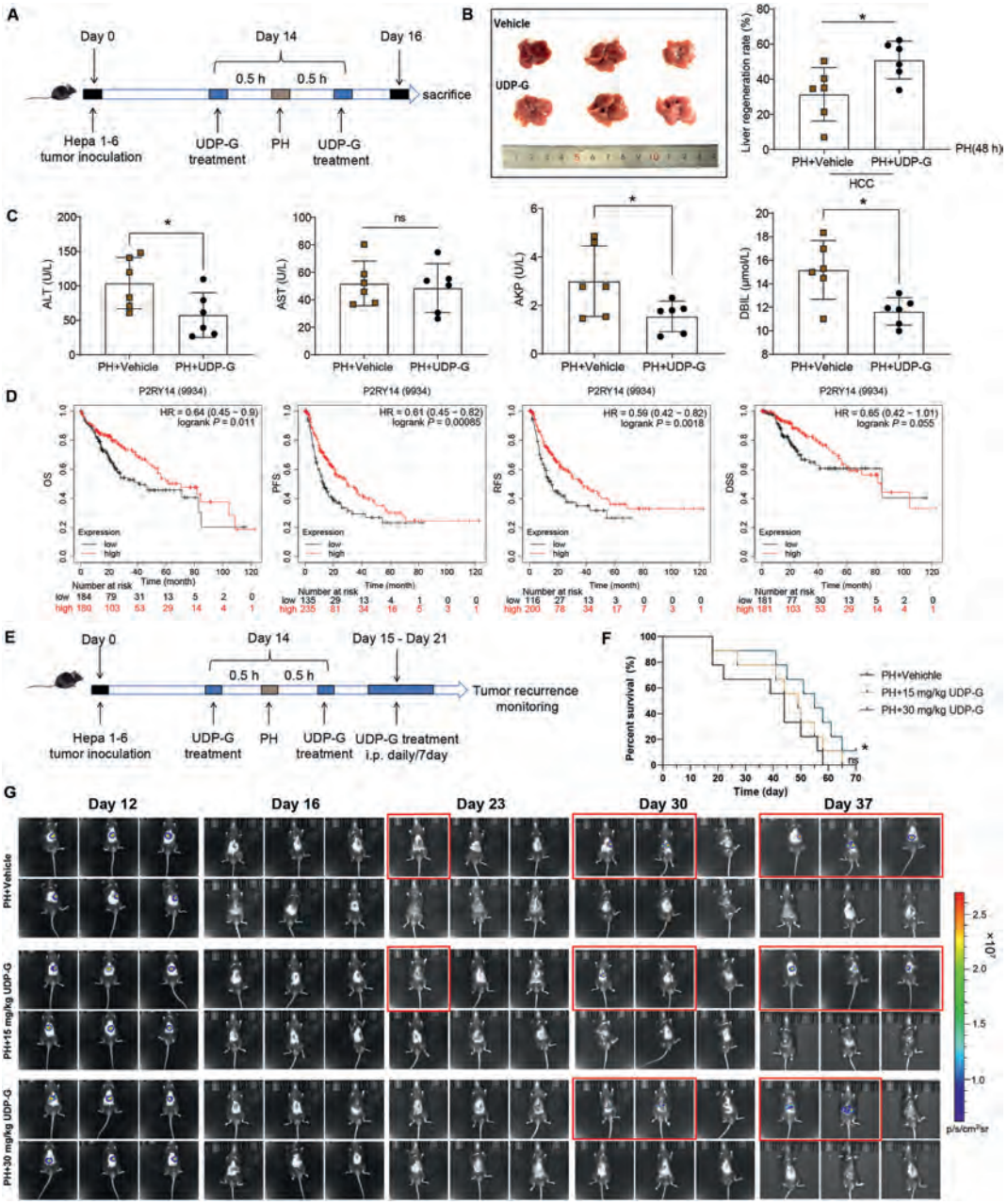

Figure 6 UDP-G treatment can promote the recovery of liver function during early-stage after hepatectomy in HCC model. (A) Schematic illustrating the schedule in therapeutic experiments with the orthotopic HCC surgical removal mouse model. (B) Gross morphology of livers and liver regeneration rate in mice after hepatectomy, $n = 6$ mice per group. (C) Level of biochemical markers related to liver function in serum of UDP-G treated mice, $n = 6$ mice per group. (D) The OS, PFS, RFS and DSS of liver cancer patients with high P2Y$_{14}$R expression. (E) Schematic illustrating the schedule in therapeutic experiments with liver cancer recurrence mouse model. (F) Cumulative survival data recorded up to 70 days, $n = 9$ mice per group. (G) Bioluminescence imaging of orthotopic HCC after removal of the primary tumors, $n = 6$ mice per group. Data are shown as the mean ± SD, $^*P < 0.05$, $^{**}P < 0.01$, $^{***}P < 0.001$. Mantel−Cox Log-rank test is conducted to show the statistical significance of the Kaplan−Meier plot. ns, no significance; AKP, alkaline phosphatase; DBIL, direct bilirubin; OS, overall survival; PFS, progression-free survival; RFS, recurrence free survival; DSS, disease-specific survival.

score of 97.0) to identify the binding sequence of CREB and DNMT3b, which was located on the forward DNA strand from nucleotides −57 to −64 (Fig. 5H). We performed ChIP assays to confirm and found that CREB bound to the promoter of DNMT3b (Fig. 5I). In summary, P2Y$_{14}$R activation by UDP-G in hepatocytes mediates CREB, which regulates the expression of DNMT3b and thus increases the methylation of Dact-2.

3.6. UDP-G treatment facilitates liver function recovery and prolongs overall survival after hepatectomy in HCC model

Hepatectomy is the best chance of cure for HCC. However, they rely on the innate ability of the liver to regenerate[28]. The above studies found that the deletion of P2Y$_{14}$R could reduce liver regeneration, so we explored the role of activating P2Y$_{14}$R in the

early post-hepatectomy stage of HCC. The animal experiment had a total duration of 16 days. We performed partial hepatectomy on Day 14 and administered 15 mg/kg UDP-G by intradermal injection. Animals were sacrificed on Day 16 and liver and blood were collected (Fig. 6A). We found that the liver regeneration rate of mice treated with UDP-G was higher than that of control group (vehicle) (Fig. 6B). The ALT, Alkaline phosphatase and DBIL levels were all significantly down-regulated in UDP-G-treated mice while AST was unchanged compared with control mice (Fig. 6C). To further confirm the relevance of $P2Y_{14}R$ with HCC, we performed a detailed analysis of RNA-Seq data from TCGA. Then we examined the relationship between the $P2Y_{14}R$ expression and clinical outcome through Kaplan−Meier Plotter[29]. The HCC patients with high $P2Y_{14}R$ expression had significantly increased overall survival, progression-free survival, recurrence free survival and disease-specific survival (Fig. 6D). These results suggest that treatment with UDP-G could increase liver regeneration and improve liver injury in postoperative recovery of early-stage HCC.

Subsequently, we investigated whether treatment with UDP-G affected overall survival and tumor size in mice with HCC. The whole animal experiment was carried out for up to 70 days (Fig. 6E). We treated mice with 15 and 30 mg/kg UDP-G respectively by intradermal injection, and found that UDP-G significantly prolonged the overall survival of the mice. Mice were all succumbed to tumors with limited survival benefits (Fig. 6F). VIS imaging began on Day 12 and ceased on Day 37 owing to the animal loss or the formation of malignant ascites (that may interfere with IVIS imaging). The results of Fig. 6G show integrated IVIS imaging data which provided visual evidence of the tumor burden. It was clear that there was no significant difference in tumor size between UDP-G treated mice and control mice (Fig. 6G). These results all reveal that UDP-G treatment could prolong the overall survival of the mice and did not affect tumor size.

4. Discussion

In ALF, the activation of liver regeneration pathway mediates hepatocyte proliferation and plays an important role in the recovery of liver function[30]. Liver regeneration contributes to regaining original size and histologic organization[31-33]. Therefore, it is of great clinical value to develop a strategy that can promote liver regeneration and the recovery of liver function for ALF patients. In the present study, we characterized the deficiency of $P2Y_{14}R$ aggravated ALF and decreased liver regeneration. Our study demonstrates a novel function of $P2Y_{14}R$ which

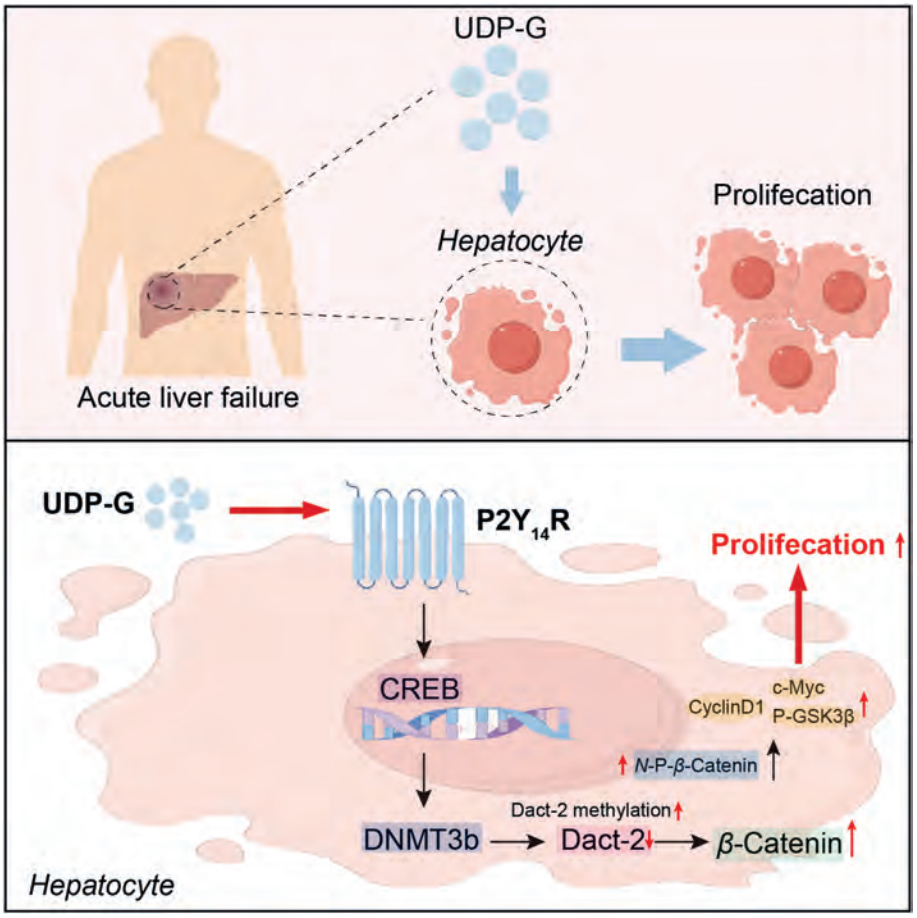

Figure 7 Schematic diagram that UDP-G/$P2Y_{14}R$ axis regulates liver pathological events. In ALF, UDP-G sensing $P2Y_{14}R$ activation could mediate DNMT3b through CREB to promote the methylation of Dact-2 and increase the expression of β-Catenin, which could facilitate liver regeneration and alleviate ALF.

accelerated liver regeneration *via* CREB/DNMT3b/Dact-2/β-Catenin signaling in ALF. This study proposes that UDP-G/$P2Y_{14}R$ axis plays an important role in promoting liver regeneration, providing a basis for drug development targeting $P2Y_{14}R$.

The previous study provided a substantial piece of evidence to further understand the link between live regeneration and disease phenotype in ALF[34]. Our study found that $P2Y_{14}R$ knockout inhibited liver β-Catenin activation, thereby inhibiting liver regeneration after ALF. Abnormal Wnt/β-Catenin signaling is not only related to the development of liver-related tumors, but also participates in the course of a variety of liver diseases such as acute liver injury, hepatitis, cirrhosis and focal nodular hyperplasia[35,36]. In recent years, the role of Wnt in the regulation of liver regeneration has attracted attention, which provides a theoretical basis for targeting Wnt therapy for liver repair after acute liver injury[37]. The natural product *Salvianolic acid A* has been reported to alleviate liver injury caused by metal accumulation by regulating SIRT1 and promoting β-Catenin signaling[38]. Then, our study found that $P2Y_{14}R$ deletion inhibits β-Catenin -mediated liver regeneration pathway through Dact-2, leading to impaired liver repair and increased liver injury. Dact binds to Dsh and stabilizes β-Catenin -degrading complex, blocking β-Catenin -mediated regeneration[39]. A study on MHCC97L cells showed that decreased expression of Dact-2 could induce G1/S phase arrest, promote cell proliferation and thus promote cell invasion[40], which is consistent with our findings. DNMT plays a catalytic and maintenance role in methylation. Among isoforms in mammals, DNMT1, DNMT3a and DNMT3b have the activity of methyl transfer[19,20]. Furthermore, we found that the mechanism by which CREB/DNMT3b/Dact-2 was involved in the regulation of liver regeneration, provided a basis for $P2Y_{14}R$-targeted treatment of ALF. As we know UDP-G could activate $P2Y_{14}R$ to mediate downstream signaling[41,42]. Interestingly, our results also show that exogenous UDP-G could promote liver regeneration after hepatectomy without affecting liver cancer recurrence, which might be the high methylation of Dact-2 and therefore liver cancer cells did not respond to UDP-G stimulation.

In our study, we discovered a new role for $P2Y_{14}R$ and elucidated the significance of its abnormal elevation in pathological processes. Different from the pro-fibrotic effect in liver fibrosis, $P2Y_{14}R$ can significantly activate the regeneration pathway during ALF to promote the recovery of liver function. Based on the findings, UDP-G sensing $P2Y_{14}R$ activation could be used for salvage in ALF or recovery of liver function after surgery with a risk of liver dysfunction. Considering the unstable metabolism of endogenous UDP-G and the short time to exert therapeutic effects, the development of long-acting agonists of $P2Y_{14}R$ or exogenous supplementation of UDP-G might be a promising candidate for ALF treatment, offering several advantages: (i) the administration of UDP-G is potentially patient safely, because of its physiological presence[43-45]; (ii) UDP-G is a distress signal after ALF, and sensing $P2Y_{14}R$ activation facilitates liver regeneration, demonstrates its feasibility in treatment of ALF; (iii) ALF patients with metabolic disturbances is the common feature, often with inhibited glucose metabolism, and exogenous UDP-G also facilitate glycogen synthesis[46]. Our findings validated that UDP-G or $P2Y_{14}R$ long-acting agonists might provide a novel treatment for ALF in humans. This work both identified a role for $P2Y_{14}R$ signaling in ALF and highlighted the administration of UDP-G to enhance liver regeneration, but there were limitations to our study. We did not identify whether UDP-G/$P2Y_{14}R$ axis played a similar role in other organs or systems rather than the liver. In astrocytes, ATP stimulates the synthesis and release of protein trophic factors and acts in combination with growth factors to stimulate proliferation[47]. Therefore, the role of UDP-G in the process of nerve injury may be worth further investigation. In summary, the present study further highlighted the importance of UDP-G/$P2Y_{14}R$ axis in liver regeneration, and provided a potential treatment strategy for ALF targeting $P2Y_{14}R$.

5. Conclusions

In conclusion, this study showed that the novel function of $P2Y_{14}R$ in acute liver failure, which could facilitate liver regeneration. Further mechanistic studies indicate that $P2Y_{14}R$ relied on CREB/DNMT3b/Dact-2/β-Catenin signaling pathway to regulate liver regeneration (Fig. 7). Additionally, the administration of exogenous UDP-G could accelerate liver regeneration and prolong the overall survival after partial hepatectomy in HCC mice. Therefore, the development of long-acting agonists of $P2Y_{14}R$ or exogenous supplementation of UDP-G may be further studied as a promising candidate for ALF treatment.

Acknowledgements

This work was supported by National Natural Science Foundation of China (No. 82373887 to Qinghua Hu, No. 82304506 to Mengze Zhou), Natural Science Foundation of Jiangsu Province (BK20211223 to Qinghua Hu, BK20231022 to Mengze Zhou, China), China Postdoctoral Science Foundation (2022M723513 to Mengze Zhou) and the Fundamental Research Funds for the Central Universities (2632024TD01 to Qinghua Hu, 2632023GR23 to Mengze Zhou, China).

Author contributions

Mengze Zhou: Visualization, Methodology, Funding acquisition, Formal analysis, Conceptualization. Yehong Li: Writing − review & editing, Writing − original draft, Visualization. Jialong Qian: Visualization, Validation, Methodology. Xinli Dong: Validation, Methodology, Data curation. Yanshuo Guo: Validation, Methodology, Data curation. Li Yin: Writing − review & editing, Visualization, Software. Chunxiao Liu: Writing − review & editing, Visualization, Methodology. Kun Hao: Resources, Project administration, Conceptualization. Qinghua Hu: Resources, Project administration, Funding acquisition, Conceptualization.

Conflicts of interest

The authors declare no conflicts of interest.

Appendix A. Supporting information

Supporting information to this article can be found online at https://doi.org/10.1016/j.apsb.2025.01.004.

References

1. Vento S, Cainelli F. Acute liver failure in low-income and middle-income countries. *Lancet Gastroenterol Hepatol* 2023;**8**:1035−45.
2. Crismale JF, Friedman SL. Acute liver injury and decompensated cirrhosis. *Med Clin North Am* 2020;**104**:647−62.

3. Angelico R, Siragusa L, Serenari M, Scalera I, Kauffman E, Lai Q, et al. Rescue liver transplantation after post-hepatectomy acute liver failure: a systematic review and pooled analysis. *Transpl Rev* 2023;**37**: 100773.
4. Shingina A, Mukhtar N, Wakim Fleming J, Alqahtani S, Wong RJ, Limketkai BN, et al. Acute liver failure guidelines. *Am J Gastroenterol* 2023;**118**:1128−53.
5. Stravitz RT, Fontana RJ, Karvellas C, Durkalski V, McGuire B, Rule JA, et al. Future directions in acute liver failure. *Hepatology* 2023;**78**:1266−89.
6. Vaughn BP, Robson SC, Burnstock G. Pathological roles of purinergic signaling in the liver. *J Hepatol* 2012;**57**:916−20.
7. Ayata CK, Ganal SC, Hockenjos B, Willim K, Vieira RP, Grimm M, et al. Purinergic P2Y₂ receptors promote neutrophil infiltration and hepatocyte death in mice with acute liver injury. *Gastroenterology* 2012;**143**:1620−29.e4.
8. Mederacke I, Filliol A, Affo S, Nair A, Hernandez C, Sun Q, et al. The purinergic $P2Y_{14}$ receptor links hepatocyte death to hepatic stellate cell activation and fibrogenesis in the liver. *Sci Transl Med* 2022;**14**:eabe5795.
9. Chen J, Zhou Y, Liu Z, Lu Y, Jiang Y, Cao K, et al. Hepatic glycogenesis antagonizes lipogenesis by blocking S1P *via* UDPG. *Science* 2024;**383**:eadi3332.
10. Mantia G, Hopps V, Leone F, Consiglio D. Effect of uridine-5-diphosphoglucose (UDPG) on liver regeneration. *Boll Soc Ital Biol Sper* 1968;**44**:260−2.
11. Freeman K, Tsui P, Moore D, Emson PC, Vawter L, Naheed S, et al. Cloning, pharmacology, and tissue distribution of G-protein-coupled receptor GPR105 (KIAA0001) rodent orthologs. *Genomics* 2001;**78**: 124−8.
12. Abbracchio MP, Boeynaems JM, Barnard EA, Boyer JL, Kennedy C, Miras Portugal MT, et al. Characterization of the UDP-glucose receptor (re-named here the $P2Y_{14}$ receptor) adds diversity to the P2Y receptor family. *Trends Pharmacol Sci* 2003;**24**:52−5.
13. Lazarowski ER, Harden TK. UDP-sugars as extracellular signaling molecules: cellular and physiologic consequences of $P2Y_{14}$ receptor activation. *Mol Pharmacol* 2015;**88**:151−60.
14. Battistone MA, Mendelsohn AC, Spallanzani RG, Allegretti AS, Liberman RN, Sesma J, et al. Proinflammatory $P2Y_{14}$ receptor inhibition protects against ischemic acute kidney injury in mice. *J Clin Invest* 2020;**130**:3734−49.
15. Liu C, Zhou M, Jiang W, Ye S, Tian S, Jiang C, et al. GPR105-targeted therapy promotes gout resolution as a switch between NETosis and apoptosis of neutrophils. *Front Immunol* 2022;**13**:870183.
16. Li H, Jiang W, Ye S, Zhou M, Liu C, Yang X, et al. $P2Y_{14}$ receptor has a critical role in acute gouty arthritis by regulating pyroptosis of macrophages. *Cell Death Dis* 2020;**11**:394.
17. Li Y, Chen J, Wang B, Xu Z, Wu C, Ma J, et al. FOXK2 affects cancer cell response to chemotherapy by promoting nucleotide *de novo* synthesis. *Drug Resist Updat* 2023;**67**:100926.
18. Wang S, Dong Y, Zhang Y, Wang X, Xu L, Yang S, et al. DACT2 is a functional tumor suppressor through inhibiting Wnt/β-catenin pathway and associated with poor survival in colon cancer. *Oncogene* 2015;**34**:2575−85.
19. Tan Y, Li QM, Huang N, Cheng S, Zhao GJ, Chen H, et al. Upregulation of DACT2 suppresses proliferation and enhances apoptosis of glioma cell *via* inactivation of YAP signaling pathway. *Cell Death Dis* 2017;**8**:e2981.
20. Cheyette BN, Waxman JS, Miller JR, Takemaru K, Sheldahl LC, Khlebtsova N, et al. Dapper, a Dishevelled-associated antagonist of beta-catenin and JNK signaling, is required for notochord formation. *Dev Cell* 2002;**2**:449−61.
21. Yin C, Evason KJ, Asahina K, Stainier DY. Hepatic stellate cells in liver development, regeneration, and cancer. *J Clin Invest* 2013;**123**: 1902−10.
22. Li W, Li L, Hui L. Cell plasticity in liver regeneration. *Trends Cell Biol* 2020;**30**:329−38.
23. Ma L, Sun H, Xu X, Chen Y, Zhang L, Li S, et al. Tumor suppressor LHPP suppresses cell proliferation and epithelial−mesenchymal transition in hepatocellular carcinoma cell lines. *J Physiol Biochem* 2022;**78**:807−17.
24. Li S, Yin L, Huang K, Zhao Y, Zhang H, Cai C, et al. Downregulation of DACT-2 by promoter methylation and its clinicopathological significance in prostate cancer. *J Cancer* 2019;**10**:1755−63.
25. Lyko F. The DNA methyltransferase family: a versatile toolkit for epigenetic regulation. *Nat Rev Genet* 2018;**19**:81−92.
26. Kausar S, Abbas MN, Cui H. A review on the DNA methyltransferase family of insects: aspect and prospects. *Int J Biol Macromol* 2021;**186**: 289−302.
27. Liu C, Wang H, Han L, Zhu Y, Ni S, Zhi J, et al. Targeting $P2Y_{14}R$ protects against necroptosis of intestinal epithelial cells through PKA/CREB/RIPK1 axis in ulcerative colitis. *Nat Commun* 2024;**15**: 2083.
28. Riddiough GE, Jalal Q, Perini MV, Majeed AW. Liver regeneration and liver metastasis. *Semin Cancer Biol* 2021;**71**:86−97.
29. Liu B, Wang T, Wang H, Zhang L, Xu F, Fang R, et al. Oncoprotein HBXIP enhances HOXB13 acetylation and co-activates HOXB13 to confer tamoxifen resistance in breast cancer. *J Hematol Oncol* 2018;**11**:26.
30. Blake MJ, Steer CJ. Liver Regeneration in acute on chronic liver failure. *Clin Liver Dis* 2023;**27**:595−616.
31. Xiang X, Feng D, Hwang S, Ren T, Wang X, Trojnar E, et al. Interleukin-22 ameliorates acute-on-chronic liver failure by reprogramming impaired regeneration pathways in mice. *J Hepatol* 2020;**72**: 736−45.
32. Kotulkar M, Paine Cabrera D, Abernathy S, Robarts DR, Parkes WS, Lin Rahardja K, et al. Role of HNF4alpha−cMyc interaction in liver regeneration and recovery after acetaminophen-induced acute liver injury. *Hepatology* 2023;**78**:1106−17.
33. Zhan C, Lin G, Huang Y, Wang Z, Zeng F, Wu S. A dopamine-precursor-based nanoprodrug for *in-situ* drug release and treatment of acute liver failure by inhibiting NLRP3 inflammasome and facilitating liver regeneration. *Biomaterials* 2021;**268**:120573.
34. Zhou J, Sun X, Chen X, Liu H, Miao X, Guo Y, et al. Phosphatidic acid-enabled MKL1 contributes to liver regeneration: translational implication in liver failure. *Acta Pharm Sin B* 2024;**14**:256−72.
35. Russell JO, Monga SP. Wnt/β-Catenin signaling in liver development, homeostasis, and pathobiology. *Annu Rev Pathol* 2018;**13**:351−78.
36. Tan K, Xie X, Shi W, Miao L, Dong X, Yang W, et al. Deficiency of canonical Wnt/β-catenin signalling in hepatic dendritic cells triggers autoimmune hepatitis. *Liver Int* 2020;**40**:131−40.
37. Khurana C, Bedi O. Proposed hypothesis of GSK-3β inhibition for stimulating Wnt/β-catenin signaling pathway which triggers liver regeneration process. *Naunyn Schmiedebergs Arch Pharmacol* 2022; **395**:377−80.
38. Shi X, Zhao Y, Ding C, Wang Z, Ji A, Li Z, et al. Salvianolic acid A alleviates chronic ethanol-induced liver injury *via* promotion of β-catenin nuclear accumulation by restoring SIRT1 in rats. *Toxicol Appl Pharmacol* 2018;**350**:21−31.
39. Choi SC, Han JK. Rap2 is required for Wnt/β-catenin signaling pathway in Xenopus early development. *EMBO J* 2005;**24**:985−96.
40. Gao S, Yang Z, Zheng ZY, Yao J, Zhang F, Wu LM, et al. Reduced expression of DACT2 promotes hepatocellular carcinoma progression: involvement of methylation-mediated gene silencing. *World J Surg Oncol* 2013;**11**:57.
41. Meister J, Le Duc D, Ricken A, Burkhardt R, Thiery J, Pfannkuche H, et al. The G protein-coupled receptor $P2Y_{14}$ influences insulin release and smooth muscle function in mice. *J Biol Chem* 2014;**289**:23353−66.
42. Sesma JI, Weitzer CD, Livraghi Butrico A, Dang H, Donaldson S, Alexis NE, et al. UDP-glucose promotes neutrophil recruitment in the lung. *Purinergic Signal* 2016;**12**:627−35.
43. Kook S, Cho J, Lee SB, Lee BC. The nucleotide sugar UDP-glucose mobilizes long-term repopulating primitive hematopoietic cells. *J Clin Invest* 2013;**123**:3420−35.

44. Ma J, Wei K, Liu J, Tang K, Zhang H, Zhu L, et al. Glycogen metabolism regulates macrophage-mediated acute inflammatory responses. *Nat Commun* 2020;**11**:1769.
45. Zhang JZ, Shi NR, Wu JS, Wang X, Illes P, Tang Y. UDP-glucose sensing $P2Y_{14}R$: a novel target for inflammation. *Neuropharmacology* 2023;**238**:109655.
46. Petersen KF, Cline GW, Gerard DP, Magnusson I, Rothman DL, Shulman GI. Contribution of net hepatic glycogen synthesis to disposal of an oral glucose load in humans. *Metabolism* 2001;**50**:598−601.
47. Rathbone MP, Middlemiss PJ, Gysbers JW, Andrew C, Herman MA, Reed JK, et al. Trophic effects of purines in neurons and glial cells. *Prog Neurobiol* 1999;**59**:663−90.